Bulletin of Faculty of Science ,Zagazig University (BFSZU) **2023**

Bulletin of Faculty of Science, Zagazig University (BFSZU)
e-ISSN: 1110-1555
Volume-2023, Issue-1, pp-24-31
Research Paper DOI: **10.21608/bfszu.2022.157337.1172**

Structural and magnetic properties of chromium substituted lithium zinc ferrite nanoparticles

A.Y. Sleem, N.I. Abu-Elsaad, S.A. Mazen

Magnetic Semiconductor Laboratory, Physics Department, Faculty of Science, Zagazig University, Zagazig, Egypt

ABSTRACT : **The structural and magnetic characteristics of $Li_{0.4}Zn_{0.2}Cr_xFe_{2.4-x}O_4$ (x = 0.0, 0.1, 0.2, 0.3, 0.4 and 0.5) ferrites produced via citrate auto-combustion were investigated. Various intriguing modifications in the values of structural factors such as lattice constant, crystallite size, and X-ray density have been detected as the Cr^{3+} concentration is raised. X-ray diffraction validated the cubic spinel structure's single phase. The lattice parameter drops as the chromium concentration rises. The wide lines suggest that the particles are nano-sized, and the crystallite size (t) was determined to be between 23 and 29 nm. The estimated crystallite size from Williamson–Hall formula decreased with Cr concentration until x=0.4 and then rises at x=0.5. After annealing the samples at 1000 °C, several magnetic characteristics were tested at ambient temperature. The magnetization M was recorded in the magnetic field up to 5500 Am^{-1}. In addition, the influence of the applied magnetic field on relative permeability (μ_r) was discussed.**

Key words: Li-Zn-Cr ferrite, XRD, Magnetic properties.

Date of Submission: 20-08-2022 Date of acceptance: 21-09-2022

I. INTRODUCTION

Soft magnetic materials are being researched and used in a number of devices as a result of technological advancements in a variety of fields. Metal–oxide nanoparticles are becoming more attractive as a result of their distinct optical, electrical, and magnetic characteristics, which differ from the bulk state. Nanocrystalline magnetic particles are gaining popularity owing to a variety of uses, including ferrofluids, magnetic medication delivery, and cancer therapy hyperthermia, etc. (Arana et al., 2013, Li et al, 2017).

The versatility of ferrospinels nanoparticles to incorporate diverse cations into their tetrahedral and octahedral positions makes them particularly fascinating. This allows for the selective enhancement of features to meet the desired uses. Ferrospinels have been examined for electronic applications due to its high permeability, excellent electrical resistivity, mechanical hardness, chemical stability, and cost efficiency (Qu et al., 2006, Kasapoglu et al., 2007). Composition and microstructure, which are subject to the technique of synthesis, impact the characteristics of ferrite nanoparticles. Lithium ferrite and modified lithium ferrites have a variety of technical uses, including cathode materials in lithium ion batteries (Wolska et al., 1997, Obrovac et al., 1998).

Spinel ferrite has the chemical formula MFe_2O_4 and is a face-centered cubic crystal with eight molecular formulas in each crystal cell (Jadhav et al., 2017, Li et al., 2014). Oxygen ions are organized in a cubic tight packing in the spinel structure. Meanwhile, in addition to 32 oxygen ions, the crystal cell contains 32 octahedral locations and 64 tetrahedral positions, of which 16 octahedral positions (B sites) and 8 tetrahedral positions (A sites) are occupied by particular metals (Li et al., 2017). In actuality, the distribution of metal ions in spinel structure is significantly more complicated, with several affecting variables.

Different ions can be used to improve the structural and magnetic characteristics of lithium zinc ferrites. Several studies on the structural, magnetic, and electrical characteristics of Li–Zn based ferrites Like Li–Zn-Ti (Gao et al., 2019), Li–Zn-Ho (Manzoor et al., 2018), Li–Zn-Sn (Zhang et al., 2019), and Li–Zn-Mo (Gao and Wang, 2019) have been published. The citrate precursor auto-combustion approach was used to make nanocrystalline Cr-doped lithium–zinc ferrite in this study. The impact of Cr substitution on structural and magnetic characteristics has been studied.

. II. Experimental Techniques

The citrate auto-combustion technique was used to produce Li-Zn ferrite nanoparticles with the chemical formula $Li_{0.4}Zn_{0.2}Cr_xFe_{2.4-x}O_4$, where x ranges from 0.0 to 0.5 in increment of 0.1. As raw materials, analytical reagent grade lithium nitrate, zinc nitrate, chromium nitrate, iron nitrate, citric acid, and ammonia were mixed in the appropriate amounts. Our latest study describes the precise preparation procedure in full (Abu-Elsaad, 2022). All of the samples' ferrite nanoparticles were softly milled for a few hours after they were created. The granular powder was then pressed into a torodial form to be measured for magnetic properties. The obtained ferrite system compacts were then annealed in air for 2 hours at 1000 °C.

The phase purity of the as-prepared nanoparticles was verified by X-ray powder diffraction (Philips X'Pert) with CuKα radiation (λ=1.54356 Å). Moreover, our latest study depicts the phase purity of annealed materials (Abu-Elsaad, 2022). At ambient temperature, magnetization was measured as a function of low magnetic field (from 0 to 5500 Am^{-1}). In our previous work, we detailed the measuring methodology and computations in great detail (Mazen and Abu-Elsaad, 2010).

III.RESLUTS And DISCUSSIONS

X-ray analysis

The XRD patterns of $Li_{0.4}Zn_{0.2}Cr_xFe_{2.4-x}O_4$ spinel ferrites (x=0.0, 0.1, 0.2, 0.3, 0.4, and 0.5) are shown in Fig. 1. When the ICDD card no. (00-038-0259) for lithium ferrite is compared, it is discovered that all of the peaks are well suited with the features of spinel structure ferrite peaks, and there are no additional impurity peaks. As shown in Fig. 1, as the content of Cr^{3+} substituted Fe^{3+} increases, the whole peak pattern progressively shifts to a high angle. This might be due to variations in the value of the lattice parameter.

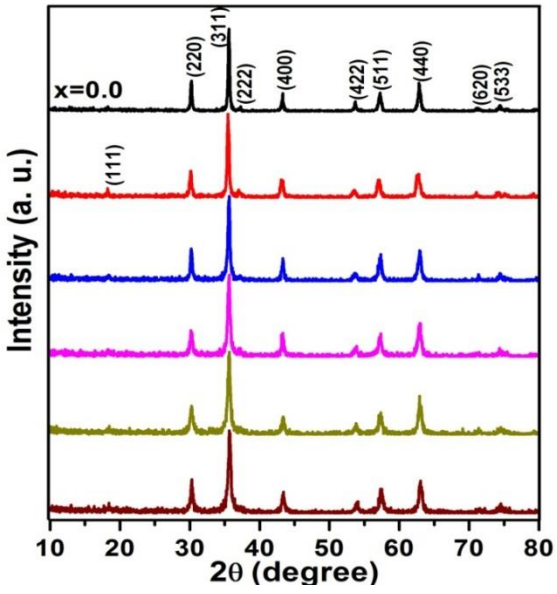

Fig. 1. XRD pattern of $Li_{0.4}Zn_{0.2}Cr_xFe_{2.4-x}O_4$ nanoparticles.

The lattice parameter was derived from the reflection planes using the equation below (Cullity, 1956):

$$a_{exp} = d_{(hkl)}\sqrt{(h^2 + k^2 + l^2)} \quad (1)$$

where, '$d_{(hkl)}$' inter-planner spacing values. For each reflection plane of the examined ferrite samples, a precise calculation of the exact lattice constant (a_{exp}) was produced using the extrapolation function F(θ), i.e., the Nelson–Riley (N–R) function (Nelson and Riley, 1945), to minimize both systematic and random errors.

$$F(\theta) = \frac{1}{2}\left[\frac{cos^2\theta}{sin\theta} + \frac{cos^2\theta}{\theta}\right] \quad (2)$$

where, θ is Bragg's angle. For any value of x, the relation depicted a straight line. The intercept on the y-axis determined the precise magnitude of the lattice constant. Fig. 2 depicts the calculated magnitudes of the lattice constant (a_{exp}) versus Cr content. The lattice parameter is shown to decrease when the chromium concentration increases. This is due to the fact that the ion radius of Cr^{3+} (0.615 Å) is less than that of Fe^{3+} (0.645 Å). As a result, substituting Cr^{3+} ions for Fe^{3+} ions reduces the lattice parameter.

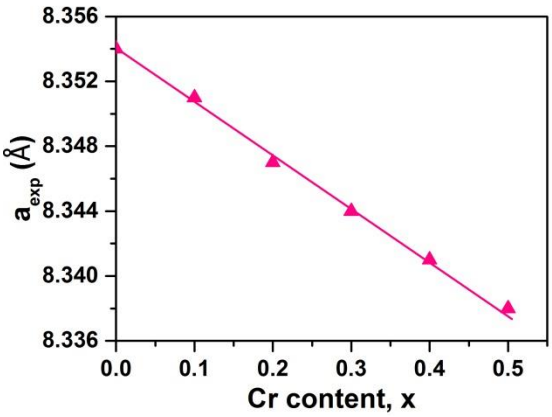

Fig. 2. Variation of lattice constant with chromium content.

The Scherrer's formula (Cullity, 1956) for the peak broadening of the six highest peaks was used to compute the average crystallite size (t_{sch}) of the specimens:

$$t_{Sch} = \frac{K\lambda}{\beta cos\theta} \quad (3)$$

where K is a form factor whose magnitude is assumed to be (0.9), λ is the wavelength of Cukα radiation, θ is the Bragg angle and β is the full-width at half maximum intensity. The crystallite sizes were calculated to be between 23 and 27 nm (Table 1).

Table 1
The lattice constant (a), crystallite size (t) and microstrain (ε) of $Li_{0.4}Zn_{0.2}Cr_xFe_{2.4-x}O_4$ ferrites.

x	a_{exp} (Å)	t_{Sch} (nm)	t_{WH} (nm)	ε	μ_{th} (μ_B) (Abu-Elsaad, 2022)
0.0	8.354	27.99	27.24	1.96	3.05
0.1	8.351	25.98	25.03	4.31	2.75
0.2	8.347	28.87	18.01	- 15.9	2.5
0.3	8.344	29.34	15.54	- 20.9	2.25
0.4	8.341	23.60	14.22	- 21.8	2
0.5	8.338	24.86	21.49	- 2.61	1.75

Furthermore, the average crystallite sizes for each sample were approximated using the Williamson–Hall formula (Williamson and Hall, 1953), with values of β cos(θ) vs. sin(θ) plotted. This results in a linear connection between β cos θ and 4 sin θ, with the intercept of the line indicating t_{WH} and the slope indicating induced strain (ε). Fig. 3 depicts representative Williamson–Hall (W–H) plots of $Li_{0.4}Zn_{0.2}Cr_xFe_{2.4-x}O_4$ (x=0.0, 0.2, 0.3, and 0.4). The crystallite size decreases with chromium concentration until x=0.4, then rises at x=0.5. Further, the discrepancy of ε shows the materials' mechanical characteristics (Table 1). Its positive value denotes tensile tensions, while negative values indicate compressive strains. This investigation on Li–Zn–Cr ferrites yields a positive value for x=0.0 and 0.1, indicating that the stresses are tensile. Meanwhile, for x≥0.2, has a negative charge, suggesting that they are compressive. This also demonstrates that by increasing the chromium level, samples change from brittle to stiff.

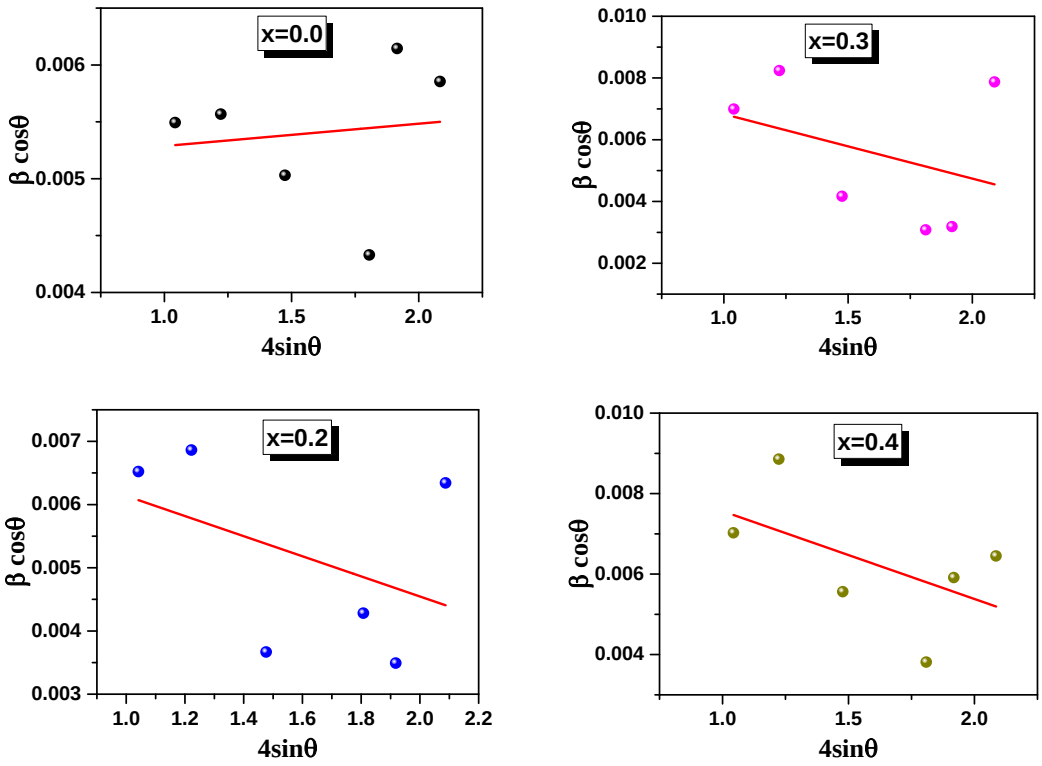

Fig. 3. W-H plot for $Li_{0.4}Zn_{0.2}Cr_xFe_{2.4-x}O_4$ (x=0.0, 0.2, 0.3 and 0.4).

Using the below relationship (**Standely, 1972)**, the magnitudes of X-ray density (d_x) were determined from the molecular weight (Mwt) and volume of the unit cell:

$$d_x = \frac{8Mwt}{Na^3} \qquad (4)$$

where N donates the Avogadro's number and a is the lattice constant (Table 1). The number 8 is used in the formula because the cubic spinel ferrite structure has eight molecules per unit cell. According to Fig. 4, the X-ray density drops with increasing Cr^{3+} concentration, which might be attributable to chromium's lower atomic mass when compared to iron.

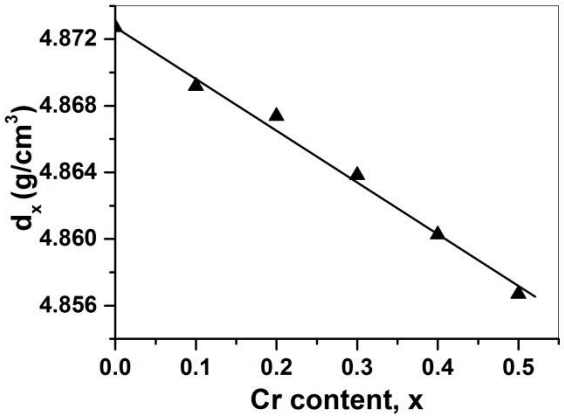

Fig. 4. Influence of Cr content on X-ray density.

Magnetic properties

The fluctuation of magnetization M with applied field intensity H for the above-mentioned composition of $Li_{0.4}Zn_{0.2}Cr_xFe_{2.4-x}O_4$ was investigated. Fig. 5a depicts the acquired results. The magnetization rises with increasing the magnetic field strength (reliant on the composition) and subsequently approaches saturation; nevertheless, the samples in the current investigation do not reach the saturation limit. The mobility of the domain borders changes their form and size when the external magnetic field H is applied. When the external field is employed, the domains try to equate in the same orientation as the field due to the motion of the domain border, and the magnetization rises as a result. As the magnetic field's strength increases, domains that are positioned in the same direction as the field direction emerge at the cost of domains that are directed in the opposite way. This technique is repeated until the magnetic field intensity is increased to the point where the macroscopic specimen converts to a single domain with roughly the same orientation as the field. Once all domains aligned with the field direction, saturation is obtained.

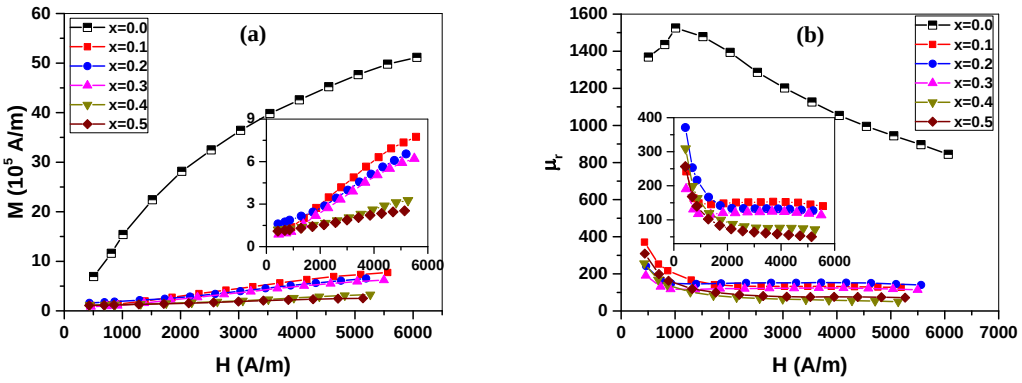

Fig. 5. The variation of (a) the magnetization (*M*) and (b) relative permeability (μ_r) of Li-Zn-Cr ferrite with the magnetizing field (*H*).

The fluctuation of relative permeability (μ_r) with the utilized magnetic field (H) for all samples is represented in Fig. 5b. The relative permeability of pure Li-Zn ferrite (x=0.0) improves as the external field rises, reaches its supreme value at lower fields (H<2000 A/m), and then drops when the applied field is increased further. Meanwhile, for x≥0.1, boosting H causes a considerable decrease in μ_r. The relative permeability (μ_r) is signified by:

$$\mu_r = \frac{B}{\mu_o H} = \frac{M}{H} + 1 \qquad (5)$$

As a result, it is dependent on the slope dM/dH. Therefore, boosting H causes a considerable decrease in μ_r. Both reversible and irreversible contributions have an impact on the amount dM/dH. The rise in μ_r can be attributed to the applied field's aligning impact on ionic spins as a result of reversible domain wall motion or reversible rotation, which causes a noticeable increase in μ_r. On the other hand, the decrease in μ_r indicates that an increase in H may generate a minor increase in B, resulting in a clear decline in μ_r.

The variation of M and μ_r with chromium content at (H = 4000 Am^{-1}) is shown in Fig. 6. It can be shown that when Cr^{3+} concentration increases, M and μ_r decrease. This variation of M is consistent with our analysis from VSM results (Abu-Elsaad, 2022). To study the behavior of magnetization vs composition x, the theoretical (effective) magnetic moment for each composition should be computed. The cation distribution of current study for Li-Zn-Cr ferrite could be represented as illustrated below (Abu-Elsaad, 2022):

$$(Zn^{2+}_{0.2-y}\ Fe^{3+}_{0.8+y})[Li^{+}_{0.4}\ Zn^{2+}_{y}\ Cr^{3+}_{x}\ Fe^{3+}_{1.6-y-x}]O_4$$

The metals in ( ) reside A location and the metals in [ ] locate B position. There are three sorts of interactions, (AA, AB and BB), AB exchange is more powerful than the others [20]. With the amount of the cations and the varied magnetic moments of the cations, the interchange between these magnetic ions will change. The magnetic moments of Li^+, Zn^{2+}, Cr^{3+}, and Fe^{3+} ions are 0 μ_B, 0 μ_B, 3 μ_B and 5 μ_B. The magnetic moment of cubic spinel ferrite may be described using Neel's model as follows (Néel, 1948):

$$|\mu_{th}(x)| = |\mu_B(x)| - |\mu_A(x)| \qquad (6)$$

μ_A and μ_B represent the magnetic moments in the A and B-sites. As can be seen, the total magnetic moment μ_{th} falls as the magnetic moments μ_A and μ_B decline. The reduction of μ_B is caused by the magnetic moment of Fe^{3+} (5 μ_B) ion replaced by Cr^{3+} (3 μ_B) at B-site. These findings are matching with our examination of VSM data (Abu-Elsaad, 2022). Table 1 shows the computed values of the overall magnetic moment (μ_{th}).

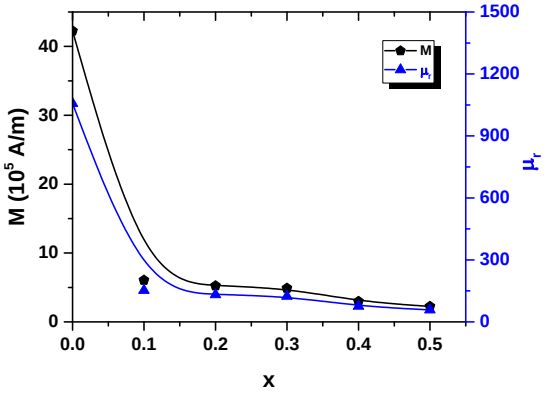

Fig.6. The variation of the magnetization (M) and relative permeability (μ_r) vs. Cr content (x) at magnetizing field (H= 4000 Am^{-1}).

Conclusions

The citrate technique was used to effectively produce the nanosized Li-Zn-Cr ferrite. The nanophase cubic spinel structure of these samples was verified by XRD patterns. The structural and magnetic characteristics of lithium zinc ferrite were significantly altered when Cr was replaced for Fe. The magnetization dropped dramatically as the Cr content increased. Neel's two sub-lattice approach

was used to investigate this phenomenon. The relative permeability shows the same magnetization tendency.

REFERENCES

Arana M., Galvan V., Jacobo S.E., Bercoff P.G. (2013): "Cation distribution and magnetic properties of LiMnZn ferrites". Journal of alloys compounds, 568: 5-10.

Li J., Peng X., Yang Y., Ge H. (2017): "Preparation and characterization of MnZn/FeSiAl soft magnetic composites". Journal of magnetism and magnetic materials, 426: 132-136.

Qu Y., Yang H., Yang N., Fan Y., Zhu H., Zou G. (2006): "The effect of reaction temperature on the particle size, structure and magnetic properties of coprecipitated $CoFe_2O_4$ nanoparticles". Materials Letters, 60: 3548-3552.

Kasapoglu N., Baykal A., Koseoglu Y., Toprak M.S. (2007): "Microwave-assisted combustion synthesis of $CoFe_2O_4$ with urea, and its magnetic characterization". Scripta Materialia, 57: 441.

Wolska E., Stempin K., Krasnowska-Hobbs O. (1997): "X-ray diffraction study on the distribution of lithium ions in $LiMn_2O_4/LiFe_5O_8$ spinel solid solutions". Solid State Ionics, 101: 527-531.

Obrovac M.N., Mao O., Dahn J.R. (1998): "Structure and electrochemistry of $LiMO_2$ (M=Ti, Mn, Fe, Co, Ni) prepared by mechanochemical synthesis", Solid State Ionics, 112: 9-19.

Jadhav J., Biswas S., Yadav A.K., Jha S.N., Bhattacharyya D. (2017): "Structural and magnetic properties of nanocrystalline Ni-Zn ferrites: in the context of cationic distribution". Journal of Alloys and Compounds, 696: 28–41.

Li L.Z., Wang R., Tu X.Q., Peng L. (2014): "Structure and static magnetic properties of Ti substituted NiZnCo ferrite thin films synthesized by the sol-gel process". Journal of Magnetism and Magnetic Materials, 355: 306–308.

Li L.Z., Zhong X.X., Wang R., Tu X.Q., Peng L. (2017): "Structural and magnetic properties of Co-substituted NiCu ferrite nanopowders". Journal of Magnetism and Magnetic Materials, 433: 98–103

Gao Yu, Wang Zhi, Shi Ruimin, Pei Jiajia, Zhang Haoming, Zhou Xueyun (2019): "Electromagnetic and microwave absorption properties of Ti doped Li-Zn ferrites". Journal of Alloys and Compounds, 805: 934-941.

Manzoor Alina, Khana Muhammad Azhar, Khan Muhammad Yaqoob, Akhtard Majid Niaz, Hussain Altaf (2018): "Tuning magnetic and high frequency dielectric behavior in Li-Zn ferrites by Ho doping". Ceramics International 44: 6321-6329.

Zhang Hao-ming, Wang Zhi, Pei Jia-jia, Gao Yu (2019): "Investigation of the structure and magnetic properties of Sn substituted Li-Zn ferrites fabricated by sol–gel process". Journal of Sol-Gel Science and Technology, 90:404–410.

Gao Yu, Wang Zhi (2019): "Effect of Mo substitution on the structural and soft magnetic properties of Li–Zn ferrites". Journal of Sol-Gel Science and Technology, 91:111–116.

Abu-Elsaad N.I., Mazen S.A., Sleem A.Y. (2022): "Production of Cr^{3+} substituted Li–Zn nanocrystalline ferrite by citrate method: Studies on structure, cation occupancy, elastic, optical and magnetic performance". Ceramics International, 48: 14210–14223.

Mazen S. A. and Abu-Elsaad N. I. (2010), Journal of Magnetism and Magnetic Materials 322: 265.

Cullity B.D. (1956): "Elements of X-ray Diffraction", Reading, Addison-Wesley Publ Comp. Inc., Massachusetts.

Nelson J.B., Riley D.P. (1945): "An experimental investigation of extrapolation methods in the derivation of accurate unit-cell dimensions of crystals". Proceedings of the Physical Society, 57: 160.

Williamson G.K., Hall W.H. (1953): "X-ray line broadening from filed aluminium and wolfram". Acta metallurgica, 1: 22–31.

Standely J. (1972): "Oxide Magnetic Materials", Clarendon.

Néel L. (1948): "Propriétés magnétiques des ferrites; ferrimagnétisme et antiferromagnétisme". In: Ann. Phys. (Paris), pp. 137–198.